Graphical Abstract

Robust Identification of Flame Frequency Response via Multi-Fidelity Gaussian Process Approach

Shuai Guo, Camilo F. Silva, Wolfgang Polifke

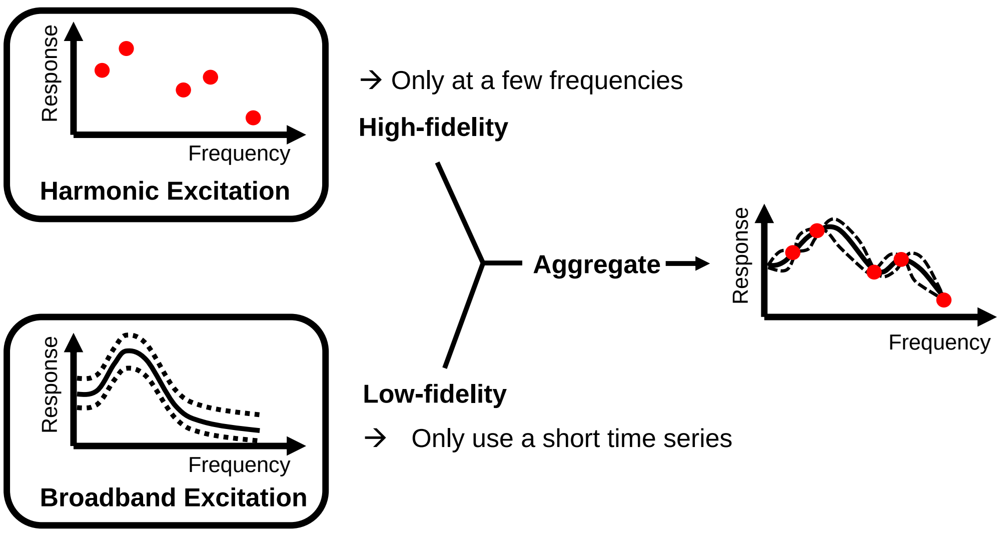

Highlights

Robust Identification of Flame Frequency Response via Multi-Fidelity Gaussian Process Approach

Shuai Guo, Camilo F. Silva, Wolfgang Polifke

- A multi-fidelity approach is proposed to identify flame frequency response in an accurate, robust and effective manner.
- Results from a short time broadband excitation (low-fidelity) and harmonic excitations at a few frequencies (high-fidelity) are aggregated.
- The proposed approach can fully exploit the respective strengths while avoiding the weaknesses of the two established identification methods.
- The proposed approach is further validated using published experimental and LES dataset of an actual test rig.

Robust Identification of Flame Frequency Response via Multi-Fidelity Gaussian Process Approach

Shuai Guo[a,*], Camilo F. Silva[a], Wolfgang Polifke[a]

[a] *Fakultät für Maschinenwesen, Technische Universität München, Boltzmannstr. 15, D-85748 Garching, Germany*

Abstract

Accurate, robust, and efficient identification of flame frequency response (FFR) plays a crucial role in thermoacoustic instability prediction, analysis and control. In order to extract the FFR from high-fidelity numerical simulation time series data, two methods are currently used in the community, which are based on harmonic excitation or broadband excitation, respectively. The former can produce quite accurate FFR estimates even in the presence of significant noise, but only at discrete frequencies; the latter method, which combines broadband forcing and system identification techniques, provides the complete FFR over the frequency range of interest, but may introduce increased levels of uncertainties in the identified results. The present study aims to fully exploit the respective strengths, while avoiding the weaknesses of the two aforementioned methods by proposing a multi-fidelity approach that merges FFR identification results from a short time broadband excitation (low-fidelity) and harmonic excitations at a few select frequencies (high-fidelity). The proposed approach is realized via a machine-

*Corresponding author:
Email address: guo@tfd.mw.tum.de (Shuai Guo)

Preprint submitted to Journal of Sound and Vibration *October 20, 2020*

learning technique called “ Multi-fidelity Gaussian Process.” Our case study demonstrates that the proposed multi-fidelity approach can effectively assimilate the global trend provided by the low-fidelity results and local estimates provided by the high-fidelity results, thus leading to a globally accurate and robust FFR identification even in the presence of strong noise. In addition, we investigate the impact of the number and locations of harmonic forcing frequencies on the performance of the proposed approach. Finally, we employ the proposed multi-fidelity framework to identify the FFR of a turbulent premixed swirl burner test rig based on previously published data, which further highlights the capability and flexibility of the proposed approach in real applications.

Keywords:
Flame frequency response, Gaussian Process, Thermoacoustic instability, Uncertainty quantification

---

1. Introduction

Common practices for investigating thermoacoustic instability in turbulent combustors involve separating the acoustic and flame aspect of the problem, where a dedicated acoustic solver (e.g., a network model [1, 2, 3] or a Helmholtz solver [4, 5, 6]) is employed to model the acoustic wave propagation and coupled with a flame model that serves as a source term in the governing equation. The flame model relates the unstead heat release rate of the flame to the flow perturbations upstream of the flame [7]. In the linear regime, this relationship is embedded in the flame frequency response (FFR), which can be understood as a transfer function that relates the spatially integrated fluctuations of heat release rate with harmonic perturbations at a given frequency of velocity at a reference location upstream of the flame [8]. The FFR can be regarded as a special case of the more general concept of flame transfer function (FTF), with evaluations only made at real-valued angular frequencies $\omega \in \mathbb{R}$ [9]. The FFR can be extended to the FTF in the complex domain [10, 11, 12, 13, 14], thus facilitating thermoacoustic instability computations and combustion noise evaluations [15, 16]. In addition, the FFR also helps to reveal the physical insights embedded in the flame responses [17, 18] and motivates designing novel robust control mechanisms [19]. Considering its central role in linear thermoacoustic instability investigations, an accurate, robust and efficient identification of FFR becomes a necessity toward achieving reliable thermoacoustic instability prediction, analysis and control.

Similar to experimental methods, the FFR can be assessed numerically by forcing the flame with harmonic signals at discrete frequencies [20]. In this approach, time series of the velocity fluctuation at a reference position upstream of the flame and of the global heat release rate are recorded. Subsequently, gain and phase of the FFR at those forcing frequencies are obtained via Fourier analysis. Although highly accurate due to the high signal-to-noise ratio (SNR), this approach can only estimate the FFR at discrete frequencies. Consequently, such an approach becomes computationally expensive when high-fidelity numerical simulations are employed and FFR values are required at many frequencies.

To overcome the above-mentioned efficiency problem, Polifke and co-workers (see [21, 8]) proposed a strategy that combines broadband excitation with advanced system identification analysis. This approach, termed *broadband excitation method* in the present study, works in the following manner: first, the CFD-simulated flame is forced with a broadband excitation signal, with low auto-correlation and constant amplitude over the range of frequencies of interest. Subsequently, the resulting fluctuations of the velocity signals u' at a reference position and the global heat release rate signals $\dot{Q}'$ are recorded. Finally, based on the this discrete input-output time series of u' and $\dot{Q}'$, system identification algorithms can be employed to derive a finite impulse response (FIR) model, which is a low-order model that characterizes the linear flame dynamics in time-domain [8]. Afterwards, the corresponding FFR can be easily obtained via applying Fourier transform to the obtained FIR model [1]. For more theoretical descriptions and practical implementations of the broadband excitation method for aero- and thermo-acoustic investigations, readers are referred to [22, 23, 24, 25, 26]. The main advantage of this method is that the complete FFR in the frequency range of interest can be obtained in "one shot," i.e., a single unsteady simulation typically lasting less than half of a second in physical time, which leads to a significant reduction in computational costs.

Note, however, that technically relevant turbulent flames often exhibit a considerable level of combustion noise, which contributes to the heat release rate fluctuation signals that is uncorrelated with excitation signal. In addition, the combustion noise is known to be colored [27, 28, 29], meaning that

[1] If the corresponding FTF is desired for the purpose of performing thermoacoustic instability computations, a z-transform of the obtained FIR model can be computed instead to achieve the goal.

it is not equally distributed over the whole frequency range. In this situation, due to the limited length of the simulated time series and the associated low SNR, this approach introduces uncertainties in the identified FFR, which may subsequently result in significant variations in thermoacoustic eigenmode calculations, thus undermining the robustness of the corresponding instability analysis [30, 31]. Although providing a longer time series to the system identification routines can alleviate the uncertainty issue, the analysis in [31] of the reduction of the identification uncertainty with time series length shows that the extra computational effort may quickly become prohibitive, which goes against the original purpose of employing the broadband excitation method. In summary, the two established methods for estimating the FFR from CFD simulations, i.e., repeated harmonic excitations or broadband excitations, are either accurate, but computationally expensive (repeated harmonic excitations), or efficient, but with considerable uncertainty if output signal noise is significant (broadband excitations).

If no single method can simultaneously satisfy requirements in terms of accuracy, robustness and efficiency, then can we obtain more favourable results via a combined strategy, which fully exploits the respective strengths, while avoiding the respective weaknesses of the individual methods? This constitutes the goal that we are pursuing in the current work. To be more specific, we are striving to answer the following question: is it possible to achieve a globally more *accurate*, *robust* and *efficient* FFR identification of turbulent flames from CFD simulations by aggregating the FFR identification results from a short-time broadband excitation with harmonic excitations at a few frequencies?

The rationale behind this question can be viewed from two perspectives: first, experience shows that a short-time broadband analysis on systems with high levels of noise, although unable to yield a quantitatively accurate FFR estimation, is sufficient to provide a qualitative description of its global trend over the frequency range of interest; meanwhile, harmonic analyses performed at selected frequencies offer quantitatively accurate, local FFR estimations, which can be effectively leveraged to fine-tune the estimated trend. Therefore, by updating the estimated global trend with highly accurate local estimations, it is now possible to identify FFR with improved global accuracy, reduced uncertainty and in a cost-effective manner.

Motivated by this new line of reasoning, we propose a *multi-fidelity* framework in the present study, where we regard the FFR identified from a *short-time* broadband excitation as the *low-fidelity* results, while treating the FFR identified via harmonic excitations at a few selected frequencies as the *high-fidelity* results. To achieve the targeted data aggregation, we employ a machine learning method called *multi-fidelity Gaussian Process* (MFGP) [32]. Special attention has been paid to the uncertainty management in the data fusion process, such that uncertainties from both fidelities are faithfully taken into account, thus reliably estimating the prediction uncertainty of the final multi-fidelity results.

To serve as a concrete first step, we adopt a thermoacoustic network model equipped with a realistic turbulent combustion noise model to generate time series [33]. In the context of the present study, the key benefits are twofold: first, the "true" FFR is known precisely (as it is simply presumed), and second, it becomes affordable to systematically assess the performance of our approach. The remainder of the paper is organized as follows. We start with a brief introduction of the employed aggregation method: multi-fidelity Gaussian Process approach, followed by a case study where we illustrate some preferable features of the proposed multi-fidelity identification strategy. We then investigate the sensitivity of the multi-fidelity results to the number and locations of the harmonic excitation frequencies. Afterward, we apply the proposed multi-fidelity framework to identify the FFR of a turbulent premixed swirl burner test rig based on previously published data. The paper closes with the main conclusions and possible directions for further study. All the code and data to reproduce the results presented in the current paper can be found at https://github.com/ShuaiGuo16/GuoSilva20c.

2. Multi-Fidelity Gaussian Process

In many instances across computational engineering, multiple computational models with varying fidelities and evaluation costs are available for the same quantity of interest. Against this background, *multi-fidelity* modeling has attracted much attention lately due to its proven track record of achieving desired prediction accuracy at a lower cost [34, 35, 36, 37]. For a comprehensive review of multi-fidelity methodology, readers are referred to [38, 39, 40, 41]. A major motive behind employing multi-fidelity strategies lies in its premise of using the low-fidelity model for quick explorations of the parameter space, while keeping the high-fidelity model in the loop to ensure accuracy [41]. In the context of the present work, we regard the FFR identified from a short-time broadband excitation as the low-fidelity results, which enables a quick glance of the general trend. Meanwhile, we treat the point estimates of FFR obtained via harmonic excitations as the high-fidelity results, which permits a refinement of the "rough" estimate of the trend yielded by the low-fidelity model. By aggregating those FFR estimates, we hope the final multi-fidelity results could be as globally accurate as the high-fidelity results, with a confidence level higher than the low-fidelity results, while requiring less computational effort than either of the approaches.

In the current work, data fusion is achieved via the multi-fidelity Gaussian Process (MFGP) approach [42]. The MFGP approach directly evolves from the fundamental Gaussian Process (GP) approach [43]: the polynomial trend term usually adopted in the fundamental GP approach is replaced by the low-fidelity approximations. In the following sections, we first discuss how to use MFGP to obtain a multi-fidelity identification of FFR. Afterward, we discuss how to derive the corresponding uncertainty.

2.1. MFGP for FFR identification

We strive to train two MFGP models for gain and phase of the FFR, respectively. In the following section, we will use gain modeling as an example. The exact same principle applies to phase modeling as well.

MFGP modeling treats the gain value G at frequency f as the realization of a Gaussian process:

$$G(f) = \beta G^{LF}(f) + Z(f) \tag{1}$$

Here, β is an unknown constant term acting as a scaling factor. $G^{LF}(f)$ represents the low-fidelity approximation of the gain-frequency relationship, and serves as the global trend term in the framework of the MFGP approach.

In our current study, this low-fidelity approximation $G^{LF}(f)$ is provided by applying the broadband excitation method as introduced above. The system identification method adopted here is the Wiener-Hopf inversion [33]. Note that other advanced system identification methods (e.g., Box-Jenkins [26]) can also be employed and integrated into the current MFGP framework.

The term $Z(f)$ corresponds to the difference between the scaled G^{LF} and G at f, which is modeled as a Gaussian stochastic function with zero mean, variance σ^2, and covariance defined as:

$$Cov[Z(f^i, f^j)] = \sigma^2 R(f^i, f^j) \tag{2}$$

where $R(f^i, f^j)$ is the correlation function between any two frequencies f^i and f^j. As suggested in [32], a cubic spline correlation function is adopted:

$$R(f^i, f^j) = \begin{cases} 1 - 15\xi^2 + 30\xi^3 & \text{for } 0 \leq \xi \leq 0.2 \\ 1.25\,(1-\xi)^3 & \text{for } 0.2 < \xi < 1 \\ 0 & \text{for } \xi \geq 1 \end{cases} \tag{3}$$

where $\xi = \theta|f^i - f^j|$ and θ is the hyperparameter that controls the level of correlation.

After creating a set of high-fidelity approximations of gain-frequency pairs, where we harmonically excite the flame at $\boldsymbol{X}_D = [f^1, ..., f^N]^T$ (training samples) and calculate their corresponding gain values $\boldsymbol{Y}_D = [G^{HF}(f^1), ..., G^{HF}(f^N)]^T$ (training sample responses), we can train the MFGP model by finding values for β, σ^2 and θ such that the likelihood of achieving the observations (training samples and their corresponding responses) is maximized. The maximum likelihood estimates of β and σ^2 can be derived analytically:

$$\widehat{\beta} = (\boldsymbol{F}^T \boldsymbol{R}_D^{-1} \boldsymbol{F})^{-1} \boldsymbol{F}^T \boldsymbol{R}_D^{-1} \boldsymbol{Y}_D \tag{4}$$

$$\widehat{\sigma^2} = \frac{1}{N} (\boldsymbol{Y}_D - \boldsymbol{F}\widehat{\beta})^T \boldsymbol{R}_D^{-1} (\boldsymbol{Y}_D - \boldsymbol{F}\widehat{\beta}) \tag{5}$$

where $\boldsymbol{R}_D$ is the N-by-N correlation matrix between frequencies in $\boldsymbol{X}_D$ and $\boldsymbol{F} = [G^{LF}(f^1), ..., G^{LF}(f^N)]^T$. For estimating θ, the following auxiliary optimization problem has to be solved:

$$\widehat{\theta} = \arg\max_{\theta} \left[-\frac{N}{2} \ln(\widehat{\sigma^2}) - \frac{1}{2} \ln(|\boldsymbol{R}_D|) \right] \tag{6}$$

Finally, the MFGP model prediction G^{MF} at an arbitrary frequency f is [32]:

$$G^{MF}(f) = \widehat{\beta} G^{LF}(f) + \boldsymbol{r}(f)^T \boldsymbol{R}_D^{-1} (\boldsymbol{Y}_D - \boldsymbol{F}\beta) \tag{7}$$

where $\boldsymbol{r}(f)$ is the correlation vector between f and all the training samples, i.e., $\boldsymbol{r}(f) = [R(f, f^1), ..., R(f, f^N)]$.

2.2. Uncertainties of FFR identification

Both uncertainties in low-high-fidelity FFR identifications should be faithfully reflected in the derivation of the multi-fidelity identification of FFR. Here, we propose a Monte Carlo procedure to propagate uncertainties in both fidelities to the final multi-fidelity identification results. To be more specific, we generate a large number of realizations (e.g., 1000) of both $G^{LF}(f)$ and $\boldsymbol{Y}_D$ according to their uncertainty descriptions, respectively. Then, for each realization of $G^{LF}(f)_{(i)}$ and $\boldsymbol{Y}_{D(i)}$, we employ the MFGP procedure to calculate their corresponding $G^{MF}(f)_{(i)}$. Subsequently, we obtain the histogram of G^{MF} at every f and extract the desired statistical indices.

In the present study, the FFR identification uncertainties associated with the broadband excitation method are directly calculated via the system identification approach [31]. For the harmonic excitation method, we derive the uncertainty of the estimated gain and phase values at one single frequency by applying a boostrapping method [10, 44] to the obtained time series of velocity and heat release rate. Note that other uncertainty derivation strategies for harmonic excitation method can also be incorporated into the proposed Monte Carlo procedure.

3. Case study

In this section, we investigate the performance of the MFGP approach by identifying the FFR of a surrogate data model characterized by a thermoacoustic network in time domain. We start by introducing the case set-up, followed by investigating the accuracy and robustness of the MFGP identification approach. Finally, we look into the sensitivity of the MFGP results to the number and locations of harmonic excitation frequencies. All the calculations are performed on an Intel Core i5-6500 CPU 3.20GHz PC.

3.1. Case set-up

We employ the thermoacoustic network model of [33] as our surrogate data model. This network model, as shown in Fig. 1, was previously used to study a turbulent swirl burner [10, 18] and can be simulated in the time

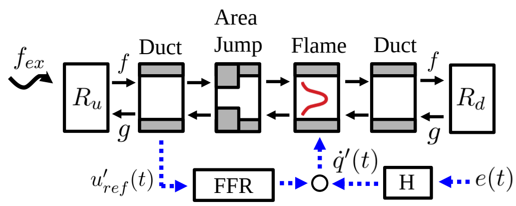

Figure 1: The employed thermoacoustic network model. f_{ex} is the external forcing wave. $u'_{ref}(t)$ and $\dot{q}'(t)$ denote the velocity fluctuation signal at the reference position and global heat release rate signal, respectively. $e(t)$ represents the noise signal.

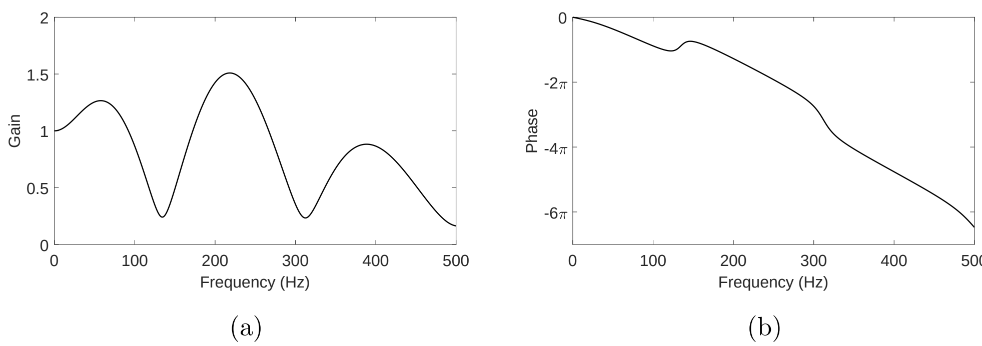

Figure 2: The reference FFR adopted in the current study.

domain [33] to generate time series for harmonic and broadband identification method.

In the context of the present study, a key benefit of this surrogate data model is that the reference FFR can be assumed *a priori*, thus allowing us to systematically assess the accuracy and robustness of the FFR identification approaches. Here, our reference FFR is depicted in Fig. 2, which represents the dynamics of a swirling flame [18], and is inserted into the "FFR" block of the network model for the subsequent time domain simulations.

Combustion noise generated by the turbulent reactive flow is modeled by using a finite impulse response filter ("H" block) applied to a white noise signal $e(t)$. This filter is obtained by fitting a finite impulse response model to the power spectral density of the combustion noise contribution (see Fig. 4 in [33]) derived from realistic LES data [10]. The signal $e(t)$ describes a random Gaussian distributed white noise signal with zero mean. After being filtered by the derived finite impulse response filter it represents the stochastic contribution to the heat release rate signal caused by combustion noise. Note that this filter is also adopted in [33, 25]. For further details on the determination of the noise model and its validation, the reader is referred to [15].

By sending in the forcing wave f_{ex} (as shown in Fig. 1), we can excite the network model and obtain the time series of reference velocity u'_{ref} and global heat release rate $\dot{q}'$. For harmonic excitation, f_{ex} is a harmonic signal oscillating at a specific frequency; for broadband excitation, f_{ex} is a pseudo random binary signal.

3.2. Characteristics of the MFGP approach

In this section, we choose one specific setting for harmonic and broadband excitation, respectively, and subsequently use MFGP to aggregate their identification results. The goal here is to illustrate the desired features of the MFGP approach in FFR identification.

In exciting the thermoacoustic network model, the f_{ex} amplitudes of both broadband and harmonic excitations are chosen such that the amplitude of $u'_{ref}(t)$ is less than 10% of the mean flow velocity. This level of excitation is generally accepted as a conservative estimate for the unset of nonlinearity. For the amplitude of noise signal $e(t)$, we assign such a value so that the

SNR value for broadband excitation equals 1, which represents a case of very high level of combustion noise. The same value of $e(t)$ for the counterpart harmonic excitation is kept. Here, expression of SNR is given as follows:

$$SNR = \frac{var(\dot{q}'_{u'})}{var(\dot{q}'_{turb})} \tag{8}$$

where $\dot{q}'_{turb}$ signal denotes the pure noise, and $\dot{q}'_{u'}$ signal denotes the heat release fluctuations resulting purely from the acoustic forcing, which is determined by simulating the network model in the time domain with a noise signal equal to zero [33]. In Eq. (8), SNR is defined as the variance ratio of the $\dot{q}'_{u'}$ signal and $\dot{q}'_{turb}$ signal.

For broadband excitation, we use a time series of 120ms, which is approximately 10 times the corresponding length of the impulse response of the adopted flame. For the present study, which relies on employing a network model (Fig. 1) to generate the required time series data, the associated computational time is negligible. However, in practice when high-fidelity CFD simulations are used to model the flame dynamics, the computational time needed to generate the time series data would be expressed in days, thus constituting the most expensive step in FFR identification procedure.

The system identification method used to post-process the broadband time series also requires negligible computational effort, i.e., 0.78s. The identified FFR is shown in Fig. 3. According to the system identification theory [45], such a short time series length, i.e., around 10 times of flame impulse response length, only satisfies the minimum requirement of time series length for the broadband excitation method to generate meaningful results. Indeed, we observe that while the identified FFR manages to capture the character-

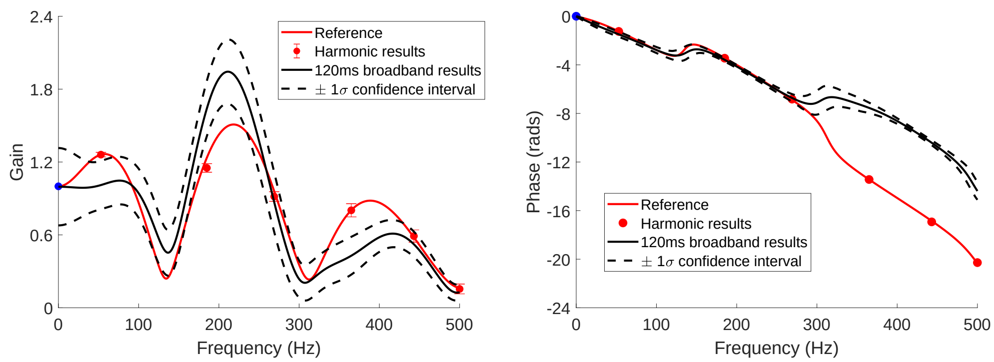

(a) (b)

Figure 3: FFR identified via a short time broadband excitation (low-fidelity results) and harmonic excitations at several frequencies (high-fidelity results). FFR values at zero frequency are known according to [46]. One standard deviation confidence intervals are also given for low-fidelity results and high-fidelity gain identification. Uncertainties of high-fidelity phase identification are negligible, and are thus not shown in the figure. High-fidelity identification provides highly accurate and certain FFR identification at selected forcing frequencies, but fails to indicate the global FFR trend.

istics of constructive/destructive interferences induced by the flame response to both swirl number fluctuations and axial velocity fluctuations, which are reflected in the location of minima and maxima in the FFR gain [18, 17], the identified FFR is not quantitatively accurate when compared with the reference FFR. Nevertheless, the obtained model qualifies for serving as the general trend in the MFGP framework.

For harmonic excitation, we choose the following six forcing frequencies as the training sample $\boldsymbol{X}_D = [53, 185, 269, 365, 443, 500]^T(Hz)$, which can properly fill the frequency range under investigation. For each forcing frequency, we generate time series with a length equal to eight times the respective oscillation period to perform the Fourier analysis. The total computational time to post-process the harmonic time series data is 36.8s, which includes both Fourier analyses and the associated bootstrapping procedures. Although the harmonic excitation method provides quantitatively accurate FFR estimates at the selected forcing frequencies, it would be difficult to deduce more than an overall low-pass behavior from these few samples of high-fidelity results. In particular, one would miss the minimum/maximum locations of the FFR gain, therefore failing to obtain further insights of the investigated flame dynamics.

By applying the MFGP approach described in section 2, we can aggregate both low- and high-fidelity results to obtain a multi-fidelity FFR identification. The total computational time is 13.6s, which includes obtaining the multi-fidelity results as well as the Monte Carlo procedure to calculate the associated uncertainty intervals. For the FFR gain estimate, as can be seen in Fig 4a, thanks to the information input from these high-fidelity samples, a significant improvement of estimation accuracy is achieved from the low-fidelity results shown in Fig. 3a. In addition, we notice that although there are no harmonic excitations applied in the frequencies that correspond to the "hill" and "valley" region of the FFR curve, the multi-fidelity approach manages to accurately reflect those features, thanks to the general trend information provided by the low-fidelity results. As for the gain estimation uncertainty, the confidence interval of the multi-fidelity results almost always covers the reference results, thus demonstrating the effectiveness of our proposed Monte Carlo procedure to account for the multi-fidelity identification uncertainty. A particularly interesting point is that, in the frequency

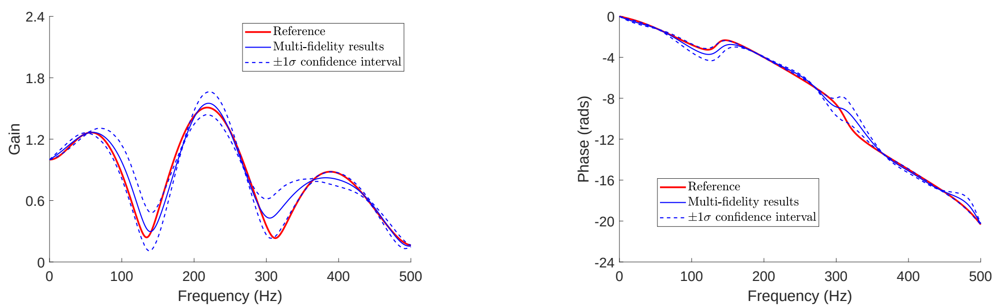

(a) (b)

Figure 4: The proposed multi-fidelity approach takes advantage of both the general trend information provided by the low-fidelity results and highly accurate local estimation information provided by the high-fidelity results, thus yielding a globally accurate and robust identification of FFR.

region where the multi-fidelity results are less accurate (e.g., $300 \sim 350Hz$ in Fig. 4a), the estimation uncertainty is also relatively large. This feature is particularly preferable as it directly indicates the frequency region with less certain predictions. Subsequently, more harmonic excitation frequencies (i.e., high-fidelity training samples) can be allocated in those regions to reduce the estimation uncertainty and improve the estimation accuracy. This demonstrates both the reliability and efficiency of the proposed multi-fidelity identification approach.

For the FFR phase estimate, we can observe similar results as the gain estimate: a good match is achieved between the estimated and the reference phase-frequency relation. In addition, the confidence interval of the multi-fidelity estimation results almost always covers the reference phase curve.

As a comparison, it would be interesting to see how accurate and robust FFR identification can be achieved by solely employing the broadband excitation method, using an equivalent total computational budget as in the MFGP approach. Here the computational budget is determined in terms of the required time series length, which can be directly translated to the core hours when CFD simulations are employed to generate the time series. The expression of the total computational budget is given as follows:

$$t_{total} = t_{LF} + \sum_{i=1}^{6}(\frac{1}{f_i} \times 8 + t_{transient}), \quad f_i \in \boldsymbol{X}_D \tag{9}$$

where t_{LF} equals 120ms. $t_{transient}$ represents the transient time each time the network model is forced, which is set to be 12ms, i.e., the impulse response length of the reference FFR. It is worth emphasizing again that the surrogate data approach adopted in the present study allows generating time series data with arbitrary length using negligible computational cost, thus facilitating systematic comparisons between various FFR identification approaches. In fact, for the purpose of the current investigation, this represents a major advantage over directly using LES to generate time series data, where every millisecond data may correspond to hundreds of core hours.

Figure 5 depicts the FFR results in this identification setting. Compared with the broadband results in Fig. 3, the longer time series improves the quality of the FFR identification. This observation is especially true for phase identification, where the accuracy and robustness are comparable to the MFGP results (Fig. 4b). However, when identifying gain, which displays more complicated frequency dependence relations compared with FFR phase, the broadband excitation method is clearly inferior to the MFGP approach. First of all, the match with the reference results in Fig. 5a degraded compared with Fig. 4a. In addition, the uncertainty interval estimated by broadband

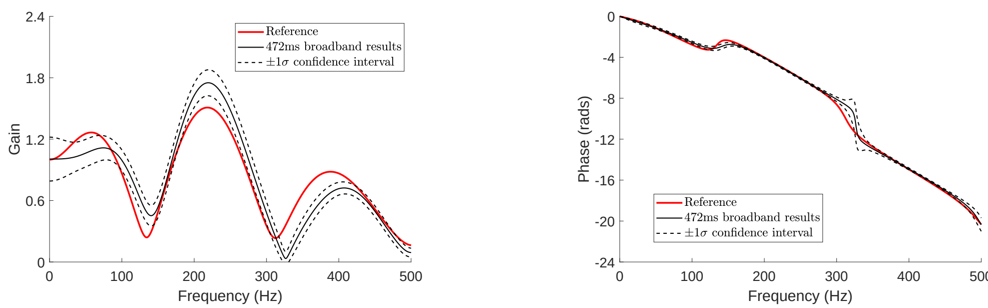

(a) (b)

Figure 5: Broadband analysis results given an equivalent computational budget as the MFGP approach. While the quality of the phase identification is comparable to MFGP approach (Fig. 4b), the broadband excitation method fails to produce as globally accurate and robust a gain identification as the MFGP approach.

excitation method is not satisfactory: gain estimate becomes overly confident in frequency regions like $100 \sim 150Hz$ and $200 \sim 400Hz$, where the confidence interval misses the reference results. In summary, for the present case study, the MFGP approach outperforms the broadband excitation method with an equivalent computational budget.

As another comparison, we use the broadband excitation method to identify FFR with a 1400ms of time series data. In this case, the time series is long enough to deliver a converged FFR identification, i.e., FFR is not changing anymore with longer time series. The obtained FFR is depicted in Fig. 6. Here, the estimated FFR does not converge towards the reference FFR. This phenomenon is induced due to the following two reasons: first, colored noise with a high level of fluctuating amplitude is presented; second, as explained in [33], the Wiener-Hopf Inversion is known to yield biased estimates in situations with feedback [47]. For the current case, the intrinsic thermoacoustic feedback cannot be avoided [48] and bias error must be expected. Compared with the multi-fidelity results shown in Fig. 4, no distinct improvements in accuracy can be observed in Fig. 6. As a matter of fact, in terms of gain identification, in frequency regions corresponding to local maxima and minima (e.g., $130Hz$, $220Hz$), multi-fidelity results actually achieve a higher accuracy, although no sampling at those frequencies are made in the multi-fidelity case. As for the uncertainty estimate, in the majority of the frequency regions, the broadband excitation method with an infinite time series length tends to yield overly confident identification results. This is especially true for the gain identification, where the confidence interval is narrow and misses the reference gain values. Since the identified FFR in Fig. 6 has already converged, it is impossible for the broadband excitation method to achieve better results, even with a longer time series. However, the multi-fidelity results presented in Fig. 4 can be further improved by allocating more forcing frequencies in the high-fidelity harmonic excitation method. This feature effectively enables a reliable FFR identification when strong noise is presented.

To summarize, by allocating computational budget for both broadband and harmonic excitations, the MFGP approach has the potential to deliver a globally more accurate and less uncertain FFR identification in the presence of strong noise, compared with solely applying the broadband excitation method given the same total computational budget.

3.3. Sensitivity of harmonic excitation setting

In this section, we investigate the impact of the harmonic excitation setting on the performance of the proposed multi-fidelity approach. To achieve

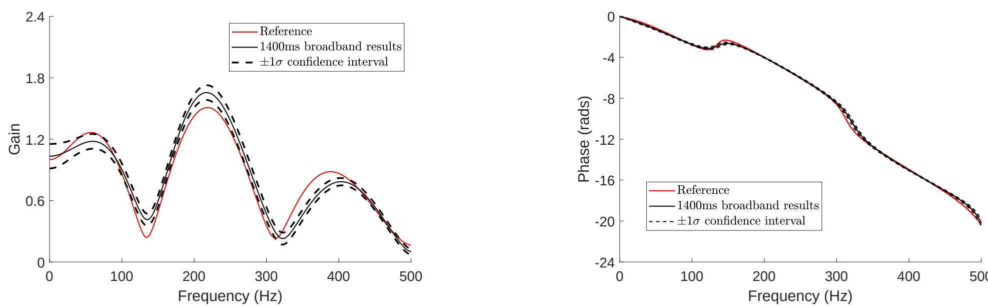

(a) (b)

Figure 6: Broadband excitation method with 1400ms time series length does not necessarily deliver a better FFR identification compared with MFGP results. For gain estimate, the local maxima and minima of the gain-frequency curve are not well captured in the presence of a high level of noise. In addition, the estimated confidence interval is too narrow to cover the reference results.

this goal, we vary the number and the locations of the exciting frequencies while maintaining the low-fidelity broadband excitation setting with 120ms of time series length. For each of these harmonic excitation settings, we carry out the corresponding FFR identifications by employing both the multi-fidelity approach and the broadband excitation method with an equivalent computational budget.

We set up four different cases with the number of forcing frequencies being 6, 7, 8 and 9, respectively, distributed within $500Hz$ range. For each case, we use the Latin-hypercube method to generate 20 random distributions of forcing frequencies. As a result, we have a total of 80 sets of harmonic forcing frequencies.

To assess the accuracy of the FFR identification methods, we calculate the associated root-mean-square-error (RMSE) between the estimated and the reference FFR gain/phase values at $f_{test} = 1Hz, 2Hz, ..., 500Hz$ and normalize it based on the range of gain/phase values, respectively, as shown in Eq. (10):

$$RMSE = \frac{\left[\frac{1}{500}\sum_{i=1}^{500}\left(\hat{y}_i - y_i^{ref}\right)\right]^{\frac{1}{2}}}{\text{range}\left(y^{ref}\right)} \tag{10}$$

where y represents gain or phase values at discrete frequencies.

In addition, we use log-likelihood (L) to measure the robustness of the FFR estimate. Based on the uncertainty information estimated by the identification method, this metric calculates the joint likelihood of obtaining the reference FFR gain/phase values at all frequencies in f_{test}, thus directly reflecting the reliablity of FFR estimation. For both the broadband and the multi-fidelity identification approach, we utilize the Matlab *ksdensity* function [49] to estimate the likelihood value at a single frequency based on the histogram of gain/phase values at that frequency, thus enabling the computation of the log-likelihood metric.

Figure 7 plots the RMSE and log-likelihood metrics for 80 multi-fidelity gain identification results. The results are grouped by the number of forcing frequencies. Within each group, the location of forcing frequencies exerts a direct impact on the performance of the multi-fidelity approach, causing the variations in accuracy and robustness. As the number of forcing frequencies increases, the multi-fidelity approach tends to yield more accurate and robust gain identification, and the performance variations induced by the locations of forcing frequency become smaller. When the number of forcing frequencies reaches 7, the multi-fidelity approach almost always outperforms the broadband excitation method with an equivalent computational budget,

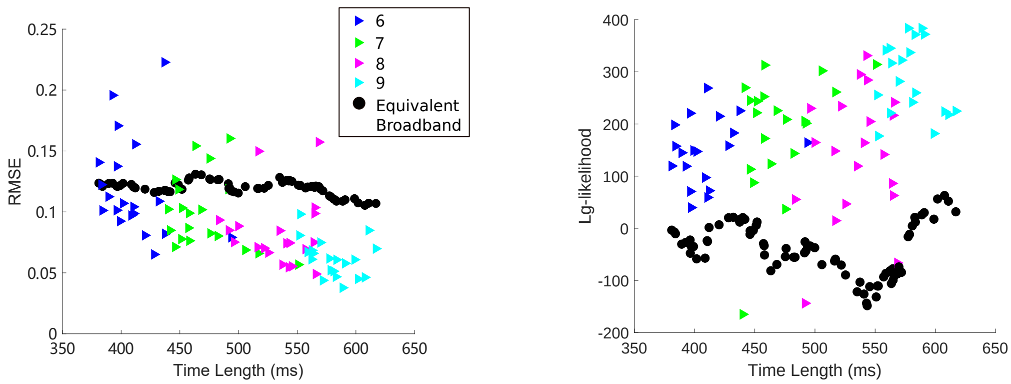

(a) (b)

Figure 7: RMSE (left, lower values are better) and log-likelihood metrics (right, higher values are better) for FFR gain estimate. Results of the MFGP identification approach are represented by triangles and they are grouped by the number of harmonic forcing frequencies. For each triangle, a corresponding broadband analysis with an equivalent computational budget is also performed and the results are depicted in circles.

achieving lower RMSE values and higher log-likelihood values.

Figure 8 plots the RMSE and log-likelihood metrics for the phase identification results. Trends similar to gain identification can also be observed in phase identification: increasing the number of harmonic forcing frequencies improves the accuracy and robustness of the multi-fidelity estimation. However, compared with the gain identification, the phase identification using MFGP yields lower RMSE values for all numbers of harmonic forcing frequencies, thus achieving a greater identification accuracy. This superior performance can be attributed to the fact that FFR phase displays a simpler relationship with respect to frequency. In comparison with the results of broadband excitation method with equivalent computational costs, when the number of harmonic forcing frequencies is low (< 8), the MFGP approach exhibits a slightly inferior identification quality, as evidenced by higher RMSE and lower log-likelihood values. The reverse is observed as more high-fidelity harmonic analysis results become available for MFGP. Notice that the broadband excitation method has already achieved an excellent FFR phase identification with a time series of 472ms (as shown in Fig. 5b). Consequently, saturations are observed both in RMSE and log-likelihood metrics of the phase identification via the broadband excitation method. In contrast, the accuracy and robustness of the MFGP results manage to maintain improving and subsequently surpassing broad results as more high-fidelity harmonic analysis results are aggregated into the multi-fidelity identification. Therefore, splitting the computational resources between both identification approaches constitutes an effective strategy to break through the "bottleneck" encountered by solely applying broadband excitation method when obtaining a reliable FFR phase identification.

4. Actual dataset application

In this section, we apply the MFGP framework to identify the FFR of a turbulent premixed swirl burner test rig by using previously published data. Toward that end, we adopt the LES broadband time series data (to estimate the FFR trend) [10], as well as the harmonic analysis data produced experimentally [18]. Originally, the FFR identified from the LES broadband time series [10] exhibited a rather high level of uncertainty due to the presence of strong combustion noise and a limited computational budget for LES (time series length was not sufficient). As a result, significant variations of the

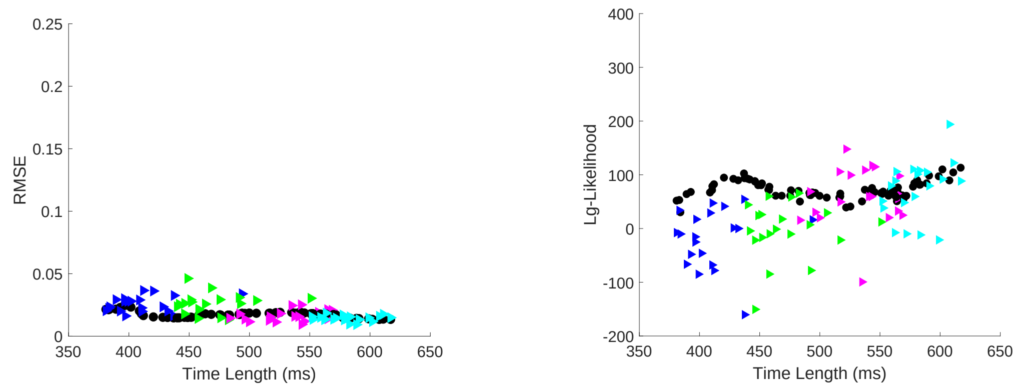

(a) (b)

Figure 8: RMSE and log-likelihood metrics for FFR phase estimate. Similar as the gain identification, more harmonic forcing frequencies lead to more accurate and less uncertain multi-fidelity phase identifications.

modal frequencies and growth rates were observed when feeding the identified FFR into the acoustic solver to predict thermoacoustic eigenmodes [31]. We show that by leveraging the accurate FFR point estimations, the MFGP strategy effectively improves the accuracy and robustness of the broadband results.

The test rig under investigation consists of a plenum, a duct with an axial swirl generator, and a combustion chamber. It operates with an equivalence ratio of 0.77 of perfectly premixed methane-air mixture and a thermal power of 30kW. Within $0 \sim 450Hz$, Komarek *et al.* [18] experimentally determined the gain/phase values at 22 discrete frequencies via harmonic analyses. Later on, Tay-Wo-Chong *et al.* [10] conducted broadband analysis on LES of the same rig, with the aim of estimating the FFR over the entire frequency range of interest. The velocity fluctuating signals (u') at the same reference

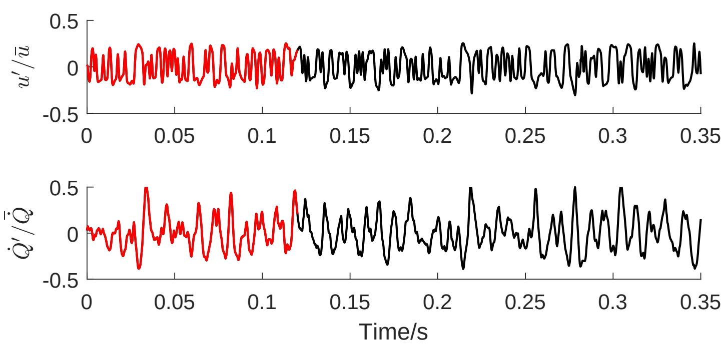

Figure 9: Recorded velocity and global heat release rate fluctuations obtained via LES forced with a broadband excitation signal. The total length of the time series is 350ms. The first 120ms (marked in red) is used to identify a low-fidelity FFR trend, which approximately amounts to 10 times the corresponding flame impulse response length.

location as the experiment were recorded, along with the global heat release rate signals ($\dot{Q}'$). A total of 350ms of time series were obtained, which are shown in Fig. 9.

To apply the proposed MFGP approach, we select the first 120ms of the recorded LES time series (Fig. 9, red lines) to estimate the low-fidelity FFR results, which are shown in Fig. 10. Since the gain-frequency relationship displayed in Fig. 10a exhibits a more complex pattern, it will be used to guide the selection of the high-fidelity harmonic estimations. In total, five forcing frequencies $f^{HF} = [100, 280, 360, 400, 440](Hz)$ are chosen, with $100Hz$ and $280Hz$ being in the vicinity of prominent gradient change of the gain-frequency curve. For a rather dense sampling choice in high frequency region ($> 300Hz$) adopted in the current case study, notice that in reality, if the harmonic analysis is performed on LES for a certain frequency, the associated computational cost would be inversely proportional to that fre-

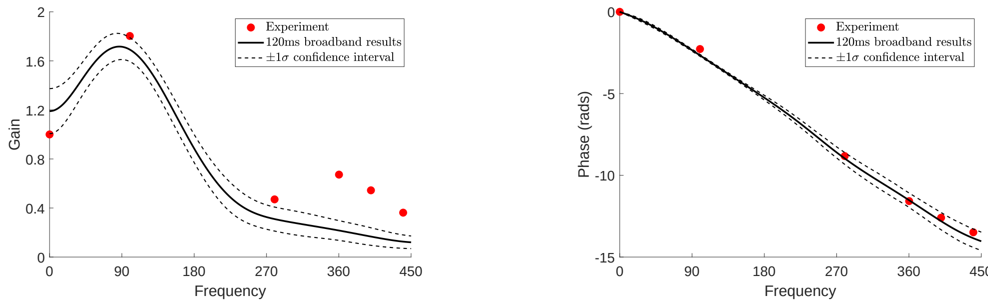

(a) (b)

Figure 10: Although a short-time broadband analysis is insufficient to provide quantitatively accurate FFR estimation, the estimated trend as well as its estimation uncertainties offer insightful guidance regarding the selection of forcing frequencies to perform harmonic analyses.

quency (Eq. (9)). Therefore, it is cost-effective to obtain more high-fidelity estimations in the high frequency region.

By aggregating the low and high-fidelity results depicted above, we obtain the multi-fidelity identification of FFR, which is shown in Fig. 11. Clearly, the information input from the harmonic analysis results has greatly improved the identification quality from the low-fidelity results, especially for the gain identification. More specifically, an excellent match is achieved between multi-fidelity estimation and experimental results, especially in the high frequency region ($> 300Hz$), where low-fidelity estimates fail to capture the bump structure induced by the constructive interference of flame responses to both swirl number and axial velocity fluctuations. In addition, the estimation uncertainty is significantly reduced compared with Fig. 10a. Nevertheless, the estimated confidence interval manages to cover the majority of the experimental results, thus yielding a very robust gain estimation.

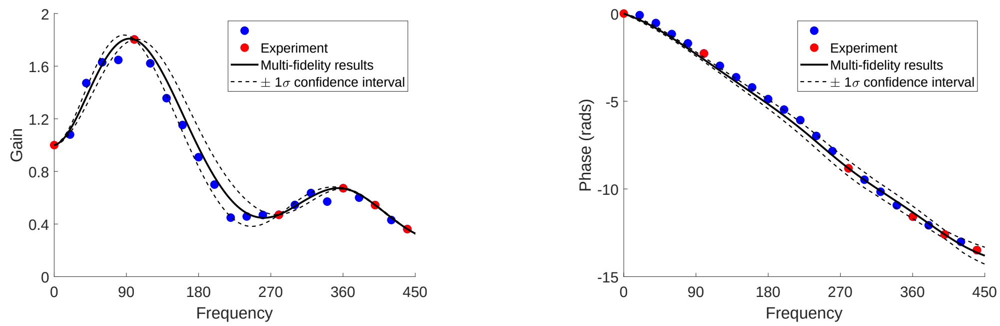

(a) (b)

Figure 11: The proposed MFGP strategy successfully aggregate the "rough" FFR trend estimated by the low-fidelity method and the highly accurate FFR point-estimations offered by the high-fidelity method, thus yielding a globally accurate and robust FFR identification. Experimental data used for training and testing are distinguished with different colored dots.

If assuming the employed experimental results in Fig. 10 are obtained via forcing the LES instead, then, by assuming using 8 cycles of time length to perform Fourier analysis on each of the excitation frequencies, the total computational cost (Eq. (9)) of the MFGP approach would be approximately equal to 350ms, i.e., the length of the full broadband time series (Fig. 9). Figure 12 shows the FFR estimation if all 350ms of time series data is fed into the broadband analysis. Clearly, for the current rig with strong turbulent combustion noise, solely relying on broadband analysis only leads to a suboptimal FFR identification. For gain estimation, a rather small increase in time series length (from 120ms to 350ms) is insufficient for capturing the second bump structure (around $360Hz$). In addition, the estimation becomes over-confident such that the calculated confidence interval fails to cover the

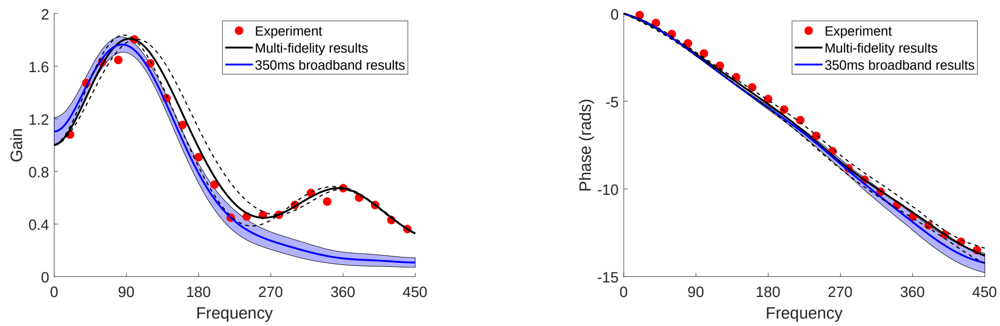

(a) (b)

Figure 12: Both multi-fidelity results and broadband results obtained by using the full time series are compared with experiments. The blue patch represents one standard deviation confidence interval of the broadband results.

majority of the experimental results. For phase estimation, the match with experimental results is not as good as the multi-fidelity results, especially in the high frequency region. In addition, the calculated confidence interval is less robust, i.e., being over-confident in lower frequency region while too conservative in the higher frequency region. To conclude, compared with solely applying broadband method, the proposed MFGP approach can potentially further increase the accuracy while lowering the uncertainty in FFR identification, especially when strong combustion noise is present.

5. Conclusion

The current study introduced a multi-fidelity approach for identifying the flame frequency response. This approach fuses FFR identification results from a short time broadband excitation (low-fidelity) and harmonic excitations at a few frequencies (high-fidelity). A *multi-fidelity Gaussian Process* technique was employed to realize the aggregation of FFR results of different fidelities. An associated Monte Carlo procedure was proposed to derive the corresponding uncertainty intervals. Our case study demonstrated that the proposed multi-fidelity approach is able to effectively assimilate the qualitatively accurate global trend provided by low-fidelity results as well as the quantitatively accurate local estimates provided by high-fidelity results, thus achieving a globally accurate, robust and efficient FFR identification, even in the presence of strong noise. We also investigated the sensitivities of the multi-fidelity identification results against the number and locations of harmonic excitation frequencies. It was shown that as the number of harmonic forcing frequencies increases, for FFR gain identification, the multi-fidelity approach, even with randomly chosen harmonic forcing frequencies, almost always outperforms the pure broadband excitation method with an equivalent computational budget; meanwhile, for phase identification, although a slightly inferior identification quality is obtained when the number of harmonic forcing frequencies is low, the multi-fidelity approach manages to keep improving the identification quality and effectively break through the accuracy and robustness bottleneck encountered by the broadband excitation approach, as more high-fidelity harmonic analysis results are aggregated into the multi-fidelity identification. Finally, we employed the multi-fidelity approach to identify the FFR of an actual turbulent swirl burner by combined use of datasets generated by LES and experiments and demonstrated the capability of the proposed approach in practical applications.

We would like to emphasize that the proposed multi-fidelity identification framework has the following features that make it especially appealing for practical applications: first, for state-of-the-art FFR identification methods, the corresponding computation effort for LES is usually at the order of millions of core hours [50]. By splitting the limited resources between both methods, we are able to combine the best of both and potentially obtain an FFR identification possessing a high level of quality, whereas the same level of quality may only be reached via high-fidelity harmonic analyses at excessive cost. The resulting reduction in computational effort would be crucial during the engine design process. Second, often simulations with harmonic forcing are carried out to study the flow physics of flame dynamics [51, 52, 53, 54, 55]. With the proposed multi-fidelity approach, the computation effort expended for this purpose can be re-used by combining with broad-band analysis, which further promotes the efficiency of this method. Third, the proposed MFGP framework is readily extendible for identifying the aero-acoustic scattering matrix of other time-invariant linear systems in aero-acoustic domains, such as a sudden area expansion of a duct [22], an orifice placed in a duct [23, 24], or acoustic resonators [56]. Fourth, the proposed MFGP framework allows experiments and simulations to go hand-in-hand, as we have demonstrated in the previous section. This is of particular importance for parametric studies, i.e. investigating FFRs at different operating conditions (e.g., equivalence ratios, power ratings, etc.): when experimental and simulation results of FFR are available at those operating conditions, MFGP could leverage on the high-fidelity experimental results to effectively reduce the modeling inadequacies of the LES (e.g., limited spatial/temporal resolution, uncertain turbulent combustion modeling, etc.), while taking advantage of the global trends offered by the broadband excitations in LES to achieve a more reliable interpolation of the experimental FFR results. Finally, in addition to the current "data-driven" model (Wiener-Hopf inversion), other "physics-informed" flame models that are tailored to specific flame domains (e.g., empirical model in [18] is specifically designed to describe swirling flames) can also be employed to serve as the general FFR trend, thanks to the flexibility offered by the proposed multi-fidelity framework. The physical knowledge injected by the empirical flame models would make multi-fidelity identification approach domain-aware, thus greatly expanding its breadth to handle various complex situations.

Further studies will focus on exploring an intelligent way to select harmonic forcing frequencies in the current multi-fidelity identification framework. For example, the frequency selection should take full advantage of the global trend information provided by the low fidelity results, e.g., choosing frequencies associated with the local minima and maxima regions, as well as regions where large uncertainties are observed.

Acknowledgments

S. Guo is grateful for the financial support from the doctoral scholarship of the Chinese Scholarship Council (No. 201606830045).

References

[1] T. Emmert, State Space Modeling of Thermoacoustic Systems with Application to Intrinsic Feedback, Ph.D. Thesis, TU München, München, Germany (2016).

[2] A. P. Dowling, The Calculation of Thermoacoustic Oscillation, Journal of Sound and Vibration 180 (4) (1995) 557–581. doi:10.1006/jsvi.1995.0100.

[3] J. J. Keller, Thermoacoustic Oscillations in Combustion Chambers of Gas Turbines, AIAA Journal 33 (12) (1995) 2280–2287. doi:10.2514/3.12980.

[4] F. Nicoud, L. Benoit, C. Sensiau, T. Poinsot, Acoustic Modes in Combustors with Complex Impedances and Multidimensional Active Flames, AIAA Journal 45 (2) (2007) 426–441. doi:10.2514/1.24933.

[5] S. M. Camporeale, B. Fortunato, G. Campa, A Finite Element Method for Three-Dimensional Analysis of Thermo-acoustic Combustion Instability, Journal of Engineering for Gas Turbines and Power 133 (1) (2011) 011506. doi:10.1115/1.4000606.

[6] P. E. Buschmann, G. A. Mensah, F. Nicoud, J. P. Moeck, Solution of Thermoacoustic Eigenvalue Problems With a Noniterative Method, Journal of Engineering for Gas Turbines and Power 142 (3) (Mar. 2020). doi:10.1115/1.4045076.

[7] L. Crocco, Aspects of Combustion Stability in Liquid Propellant Rocket Motors Part1: Fundamentals. Low frequency instability with monopropellants, Journal of the American Rocket Society 21 (6) (1951) 163–178. doi:10.2514/8.4393.

[8] W. Polifke, Black-Box System Identification for Reduced Order

Model Construction, Annals of Nuclear Energy 67C (2014) 109–128. doi:10.1016/j.anucene.2013.10.037.

[9] W. Polifke, Modeling and Analysis of Premixed Flame Dynamics by Means of Distributed Time Delays, Prog. Energy Combust. Sci. 79 (2020) 100845. doi:10.1016/j.pecs.2020.100845.

[10] L. Tay-Wo-Chong, S. Bomberg, A. Ulhaq, T. Komarek, W. Polifke, Comparative Validation Study on Identification of Premixed Flame Transfer Function, J. of Eng. Gas Turbines Power 134 (2) (2012) 021502–1–8. doi:10.1115/1.4004183.

[11] M. Schmid, R. Blumenthal, M. Schulze, W. Polifke, T. Sattelmayer, Quantitative Stability Analysis Using Real Frequency Response Data, Journal of Engineering for Gas Turbines and Power 135 (12) (2013) 121601. doi:10.1115/1.4025299.

[12] M. A. Macquisten, M. Whiteman, S. R. Stow, A. J. Moran, Exploitation of Measured Flame Transfer Functions for a Two-Phase Lean Fuel Injector to Predict Thermoacoustic Modes in Full Annular Combustors, in: Volume 4A: Combustion, Fuels and Emissions, American Society of Mechanical Engineers, Düsseldorf, Germany, 2014, p. V04AT04A003. doi:10.1115/GT2014-25036.

[13] A. Orchini, S. J. Illingworth, M. P. Juniper, Frequency domain and time domain analysis of thermoacoustic oscillations with wave-based acoustics, Journal of Fluid Mechanics 775 (2015) 387–414. doi:10.1017/jfm.2015.139.

[14] A. Orchini, Modelling and analysis of nonlinear thermoacoustic systems using frequency and time domain methods, Ph.D. thesis, University of Cambridge (2017).

[15] C. F. Silva, M. Merk, T. Komarek, W. Polifke, The Contribution of Intrinsic Thermoacoustic Feedback to Combustion Noise and Resonances of a Confined Turbulent Premixed Flame, Combustion and Flame 182 (2017) 269–278. doi:10.1016/j.combustflame.2017.04.015.

[16] C. F. Silva, P. Pettersson, G. Iaccarino, M. Ihme, Uncertainty quantification of combustion noise by generalized polynomial chaos and state-space models, Combustion and Flame 217 (2020) 113–130. doi:10.1016/j.combustflame.2020.03.010.

[17] S. Candel, D. Durox, T. Schuller, J. F. Bourgouin, J. P. Moeck, Dynamics of Swirling Flames, Annual Review of Fluid Mechanics 46 (1) (2014) 147–173. doi:10.1146/annurev-fluid-010313-141300.

[18] T. Komarek, W. Polifke, Impact of Swirl Fluctuations on the Flame Response of a Perfectly Premixed Swirl Burner, Journal of Engineering for Gas Turbines and Power 132 (6) (2010) 061503. doi:10.1115/1.4000127.

[19] S. Guo, C. F. Silva, W. Polifke, Efficient Robust Design for Thermoacoustic Instability Analysis: A Gaussian Process Approach, Journal of Engineering for Gas Turbines and Power 142 (3) (Mar. 2020). doi:10.1115/1.4044197.

[20] A. Kaufmann, F. Nicoud, T. Poinsot, Flow Forcing Techniques for Nu-

merical Simulation of Combustion Instabilities, Combustion and Flame 131 (4) (2002) 371–385. doi:10.1016/S0010-2180(02)00419-4.

[21] W. Polifke, A. Poncet, C. O. Paschereit, K. Döbbeling, Reconstruction of Acoustic Transfer Matrices by Instationary Computational Fluid Dynamics, J. of Sound and Vibration 245 (3) (2001) 483–510. doi:10.1006/jsvi.2001.3594.

[22] S. Föller, W. Polifke, Identification of Aero-Acoustic Scattering Matrices from Large Eddy Simulation: Application to a Sudden Area Expansion of a Duct, Journal of Sound and Vibration 331 (13) (2012) 3096–3113. doi:10.1016/j.jsv.2012.01.004.

[23] R. Lacombe, S. Föller, G. Jasor, W. Polifke, Y. Aurégan, P. Moussou, Identification of aero-acoustic scattering matrices from large eddy simulation: Application to whistling orifices in duct, Journal of Sound and Vibration 332 (20) (2013) 5059–5067. doi:http://dx.doi.org/10.1016/j.jsv.2013.04.036.

[24] C. Sovardi, S. Jaensch, W. Polifke, Concurrent Identification of Aero-acoustic Scattering and Noise Sources at a Flow Duct Singularity in low Mach Number Flow, J. Sound Vibration 377 (2016) 90–105. doi:10.1016/j.jsv.2016.05.025.

[25] M. Merk, S. Jaensch, C. Silva, W. Polifke, Simultaneous Identification of Transfer Functions and Combustion Noise of a Turbulent Flame, J. Sound Vibration 422 (2018) 432–452. doi:10.1016/j.jsv.2018.02.040.

[26] M. Merk, R. Gaudron, C. Silva, M. Gatti, C. Mirat, T. Schuller, W. Polifke, Prediction of Combustion Noise of an Enclosed Flame by Simultaneous Identification of Noise Source and Flame Dynamics, Proceedings of the Combustion Institute 37 (2019) 5263–5270. doi:10.1016/j.proci.2018.05.124.

[27] H. A. Hassan, Scaling of combustion-generated noise, Journal of Fluid Mechanics 66 (03) (1974) 445. doi:10.1017/S0022112074000292.

[28] S. Kotake, K. Takamoto, Combustion Noise: Effects of the Shape and Size of Burner Nozzle, Journal of Sound and Vibration 112 (2) (1987) 345–354. doi:10.1016/S0022-460X(87)80201-8.

[29] R. Rajaram, T. Lieuwen, Acoustic radiation from turbulent premixed flames, Journal of Fluid Mechanics 637 (2009) 357–385. doi:10.1017/S0022112009990681.

[30] S. Guo, C. F. Silva, M. Bauerheim, A. Ghani, W. Polifke, Evaluating the impact of uncertainty in flame impulse response model on thermoacoustic instability prediction: A dimensionality reduction approach, Proceedings of the Combustion Institute 37 (2019) 5299–5306. doi:10.1016/j.proci.2018.07.020.

[31] S. Guo, C. F. Silva, A. Ghani, W. Polifke, Quantification and Propagation of Uncertainties in Identification of Flame Impulse Response for Thermoacoustic Stability Analysis, J. Eng. Gas Turbines and Power 141 (2) (2019) 021032–10. doi:10.1115/1.4041652.

[32] Z.-H. Han, S. Görtz, Hierarchical Kriging Model for Variable-Fidelity Surrogate Modeling, AIAA Journal 50 (9) (2012) 1885–1896. doi:10.2514/1.J051354.

[33] S. Jaensch, M. Merk, T. Emmert, W. Polifke, Identification of Flame Transfer Functions in the Presence of Intrinsic Thermoacoustic Feedback and Noise, Combustion Theory and Modelling 22 (3) (2018) 613–634. doi:10.1080/13647830.2018.1443517.

[34] L. L. Gratiet, Recursive co-kriging model for design of computer experiments with multiple levels of fidelity, International Jounral for Uncertainty Quantification 4 (5) (2014) 365–386. doi:10.1615/Int.J.UncertaintyQuantification.2014006914.

[35] L. W. T. Ng, K. E. Willcox, Multifidelity approaches for optimization under uncertainty, International Journal for Numerical Methods in Engineering 100 (10) (2014) 746–772. doi:10.1002/nme.4761.

[36] J. de Baar, S. Roberts, R. Dwight, B. Mallol, Uncertainty quantification for a sailing yacht hull, using multi-fidelity kriging, Computers & Fluids 123 (2015) 185–201. doi:10.1016/j.compfluid.2015.10.004.

[37] P. S. Palar, T. Tsuchiya, G. T. Parks, Multi-fidelity non-intrusive polynomial chaos based on regression, Computer Methods in Applied Mechanics and Engineering 305 (2016) 579–606. doi:10.1016/j.cma.2016.03.022.

[38] D. J. J. Toal, Some considerations regarding the use of multi-fidelity Kriging in the construction of surrogate models, Structural and Multi-

disciplinary Optimization 51 (6) (2015) 1223–1245. doi:10.1007/s00158-014-1209-5.

[39] M. G. Fernández-Godino, C. Park, N.-H. Kim, R. T. Haftka, Review of multi-fidelity models, arXiv:1609.07196 [stat] (Sep. 2016). arXiv:1609.07196.

[40] C. Park, R. T. Haftka, N. H. Kim, Remarks on multi-fidelity surrogates, Structural and Multidisciplinary Optimization 55 (3) (2017) 1029–1050. doi:10.1007/s00158-016-1550-y.

[41] B. Peherstorfer, K. Willcox, M. Gunzburger, Survey of Multifidelity Methods in Uncertainty Propagation, Inference, and Optimization, SIAM Review 60 (3) (2018) 550–591. doi:10.1137/16M1082469.

[42] I. Abdallah, C. Lataniotis, B. Sudret, Parametric hierarchical kriging for multi-fidelity aero-servo-elastic simulators — Application to extreme loads on wind turbines, Probabilistic Engineering Mechanics (Oct. 2018). doi:10.1016/j.probengmech.2018.10.001.

[43] P. Chattopadhyay, S. Mondal, A. Ray, A. Mukhopadhyay, Dynamic Data-Driven Combustor Design for Mitigation of Thermoacoustic Instabilities, Journal of Dynamic Systems, Measurement, and Control 141 (1) (2018) 014501–014501–7. doi:10.1115/1.4040210.

[44] B. Efron, R. Tibshirani, An Introduction to the Bootstrap, Chapman & Hall, 1993.

[45] A. K. Tangirala, Principles of System Identification: Theory and Practice, CRC Press, Boca Raton, FL, 2014.

[46] W. Polifke, C. J. Lawn, On the Low-Frequency Limit of Flame Transfer Functions, Combustion and Flame 151 (3) (2007) 437–451. doi:10.1016/j.combustflame.2007.07.005.

[47] L. Ljung, System Identification: Theory for the User, 2nd Edition, Prentice Hall PTR, New Jersey, 1999.

[48] S. Bomberg, T. Emmert, W. Polifke, Thermal Versus Acoustic Response of Velocity Sensitive Premixed Flames, Proceedings of the Combustion Institute 35 (3) (2015) 3185–3192. doi:10.1016/j.proci.2014.07.032.

[49] H. P. D, Kernel estimation of a distribution function, Communications in Statistics - Theory and Methods 14 (3) (1985) 605–620. doi:10.1080/03610928508828937.

[50] M. Merk, C. Silva, W. Polifke, R. Gaudron, M. Gatti, C. Mirat, T. Schuller, Direct Assessment of the Acoustic Scattering Matrix of a Turbulent Swirl Combustor by Combining System Identification, Large Eddy Simulation and Analytical Approaches, J. Eng. Gas Turbines and Power 141 (2) (2019) 021035–021035–9. doi:10.1115/1.4040731.

[51] T. Poinsot, D. Veynante, Theoretical and Numerical Combustion, 3rd Edition, CNRS, Paris, 2012.

[52] S. Hermeth, G. Staffelbach, L. Y. M. Gicquel, T. Poinsot, LES evaluation of the effects of equivalence ratio fluctuations on the dynamic flame response in a real gas turbine combustion chamber, Proceedings of the Combustion Institute 34 (2) (2013) 3165–3173. doi:10.1016/j.proci.2012.07.013.

[53] M. Blanchard, T. Schuller, D. Sipp, P. J. Schmid, Response Analysis of a Laminar Premixed M-Flame to Flow Perturbations Using a Linearized Compressible Navier-Stokes Solver, Physics of Fluids 27 (4) (2015) 043602. doi:10.1063/1.4918672.

[54] X. Han, J. Yang, J. Mao, LES investigation of two frequency effects on acoustically forced premixed flame, Fuel 185 (2016) 449–459. doi:10.1016/j.fuel.2016.08.005.

[55] A. Ghani, L. Gicquel, T. Poinsot, Acoustic Analysis of a Liquid Fuel Swirl Combustor Using Dynamic Mode Decomposition, in: ASME Turbo Expo 2015: Turbine Technical Conference and Exposition, American Society of Mechanical Engineers Digital Collection, 2015. doi:10.1115/GT2015-42769.

[56] K. Förner, W. Polifke, Aero-Acoustic Characterization of Helmholtz Resonators in the Linear Regime with System Identification, in: 22nd International Congress on Sound and Vibration (ICSV22), Florence, Italy, 2015.